Journal of Magnetic Resonance **153,** 178–185 (2001)
doi:10.1006/jmre.2001.2450, available online at http://www.idealibrary.com on IDEAL®

Multifrequency Probe for Pulsed EPR and ENDOR Spectroscopy

Nikolai I. Avdievich[1] and Gary J. Gerfen

Department of Physiology and Biophysics, Albert Einstein College of Medicine, 1300 Morris Park Avenue, Bronx, New York 10461

Received December 20, 2000; revised September 10, 2001; published online November 7, 2001

The design, construction, and performance of a multifrequency pulsed EPR and ENDOR probe for use at cryogenic temperatures are described. Interchangeable resonators based on a folded strip line design allow variation of the resonance frequency over a range of 5–11 GHz. Variable coupling to the resonator is achieved capacitively via a simple mechanical adjustment which is thermally and mechanically stable. The entire assembly is robust and easily fabricated. Common methods of analyzing the resonator parameters such as the *Q*-factor and coupling coefficient are discussed quantitatively. Probe performance data and multifrequency pulsed ENDOR spectra are presented. © 2001 Elsevier Science

Key Words: **EPR instrumentation; pulsed ENDOR; ESEEM; resonator; coupling measurement.**

INTRODUCTION

Multifrequency pulsed electron paramagnetic resonance (EPR) involves the acquisition of electron spin-echo envelope modulation (ESEEM) patterns (*1*) and electron nuclear double resonance (ENDOR) spectra (*2*) as a function of microwave excitation frequency. Parametric variation of the EPR frequency, and corresponding resonant magnetic field strength, influences ESEEM/ENDOR spectral characteristics in a way that enhances both the detection of spectral transitions and the determination of electron-nuclear spin Hamiltonian parameters (*3*). Multifrequency ESEEM/ENDOR has been used to track the field-dependent spectral frequencies to determine accurately nuclear spin coupling constants (*4*), increase the ESEEM amplitude of coupled nuclei and therefore increase signal-to-noise ratios (*5*), and vary spectral linewidths to maximize spectral information content and to overcome the limitations imposed by instrumental deadtime (*6*).

The range over which the EPR frequency may be usefully varied normally lies outside the bandwidth of the microwave resonant structure and potentially outside the bandwidth of typical spectrometer components. The requirement for excitation and detection over a range encompassing several GHz has led to a continuing effort to develop spectrometers and microwave resonators which facilitate multifrequency operation.

[1] To whom correspondence should be addressed. E-mail: navdievi@aecom.yu.edu.

The pulsed EPR method imposes specific demands on microwave resonators used to confine the alternating magnetic field required for electron spin nutation. The features of great importance are a low-loaded quality factor (Q_L) and a high filling factor (η). A low Q_L establishes the high time resolution ($\sim$100 ns) of the method by decreasing the measurement dead time due to the cavity ringing and increasing the cavity bandwidth ($\Delta\omega = \omega_0/Q_L$) to admit narrow (10–100 ns) microwave pulses. The high filling factor maximizes sensitivity and minimizes the applied power required to obtain optimal spin flip angles. Several types of microwave structures satisfying these requirements have been described (including their potential and/or actual implementation as multifrequency devices): slotted tube (STR) (*7*), loop-gap (LGR) (*8–10*), bridged loop-gap (BLGR) (*11*), dielectric (*12*), strip line (*13*), folded strip line (*14*), and transmission line (*15*) resonators. Another important aspect of microwave cavity design is the coupling mechanism. For the majority of pulsed EPR applications, it is well known that the low Q_L should be obtained by overcoupling rather than by simply decreasing the unloaded Q_U value (*16, 17*). The coupler should be thermally and mechanically stable and provide sufficient dynamic range to reach overcoupling. A broadband coaxial coupler in combination with an antenna loop is commonly used to introduce microwave power into ST and LG resonators (*8, 10, 11*). A drawback of this type of coupling is susceptibility to vibration, which can make inductive coupling unreliable when used at low temperatures. Waveguide coupling (*13, 14, 18*), which is intrinsically robust, limits the system bandwidth. Here we describe a multifrequency ESEEM/ENDOR probe whose resonant frequency can be precisely and easily set in the range of 5–11 GHz and which provides stable, remotely adjustable capacitive coupling over a temperature range of 2–300 K.

PROBE DESIGN AND CONSTRUCTION

To meet the demands of low Q_L, high η, stable coupling, and multifrequency capability, we based the probe design on the folded half-wave resonator described by Lin *et al*. (*14*). This resonant structure consists of a slotted ring with a circumference equal to $\lambda/2$. In contrast to an LGR, the resonance frequency of this resonator is almost entirely determined by the length of the

1090-7807/01 $35.00

strip and does not depend on the gap size. Certainly this type of resonant structure lacks a well-defined separation of electric and magnetic components of the microwave field (a major advantage of LGR), which makes it inappropriate for studies involving polar liquid state samples. However, ESEEM and ENDOR are commonly performed on frozen solution samples at cryogenic temperatures, conditions under which the dielectric loss of the sample is not a significant factor. As has been described (*14*) the resonator has a high filling factor and an unloaded Q_U of about 1000. These features together with the ease of construction and frequency adjustment make this resonator very attractive for use in multifrequency pulsed EPR experiments.

The limited space of an immersion liquid N_2/He dewar and the requirement of significant bandwidth led to the choice of a coaxial coupling mechanism. As noted above, low temperature conditions of liquid cryogen immersion systems require a high degree of thermal and mechanical stability of this microwave coupling scheme.

Figure 1 illustrates the design of the pulsed EPR probe. The folded strip line resonator was cut from aluminum or silver foil, placed on the top of a Teflon holder-A, and fastened by wrapping with a thin strip of Teflon tape. The vertical size of the metal strip measures 6 mm. The holder, with the resonator attached, is inserted into a cylindrical gold-plated brass microwave shield, which acts as a waveguide beyond cutoff and suppresses all undesirable modes. Gold plating over silver plating was used to eliminate an artifact signal near $g = 2$ produced by the brass microwave shield. The holder-A is attached to a stainless steel tube, which serves as a sample guide and allows the exchange of samples during an experiment. The inner diameter of the sample guide tube (5.3 mm) is large enough to accommodate sample tubes up to 5 mm in size, which can be used for lower (C-band) frequency experiments. A stainless steel tube of larger diameter (o.d. 9.5 mm) is placed over the sample guide tube and attached to the cover brass flange to protect against mechanical stress. Microwave power is introduced into the resonator using copper (o.d. 0.25 in. and 0.141 in.) and stainless steel (o.d. 0.141 in.) semi-rigid coaxial cables connected to an SMA female elbow receptacle connector which, in turn, is attached to the microwave shield. The coaxial line running the length of the probe consists of three separate pieces with a central stainless steel thermal conductivity block section for the purpose of decreasing heat leakage. The central conductor of the receptacle connector extends into the microwave shield and provides capacitive coupling to the strip line resonator. Rotation of the stainless steel sample guide tube at the top of the probe changes the position of the folded strip with respect to the central conductor and thus varies the coupling to the resonator. Four possible positions of the strip corresponding to no coupling ($\beta = 0$), critical coupling ($\beta = 1$), and overcoupling ($\beta > 1$) are shown in Fig. 2. The coupling mechanism can be depicted as two capacitors connecting the central conductor to each end of the inductive loop. When these capacitors are equal the coupling is minimized (Figs. 2A and 2B).

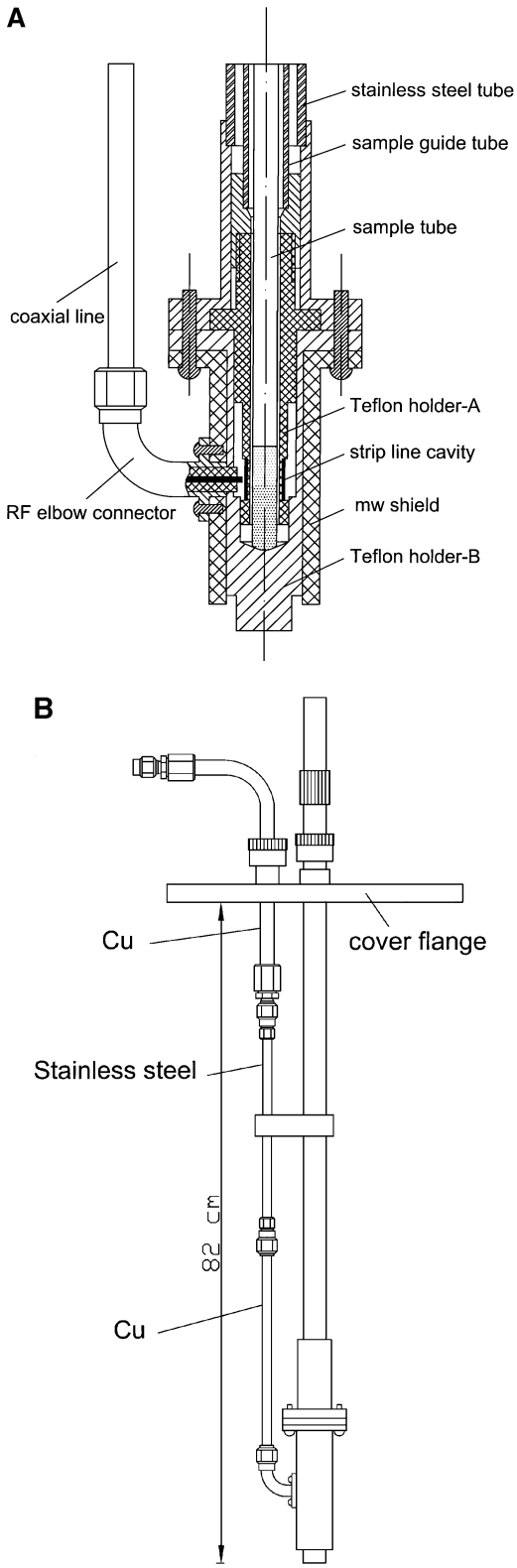

FIG. 1. (A) Longitudinal cross section of the lower part of the pulsed EPR probe. (B) Diagram of the entire pulsed EPR probe.

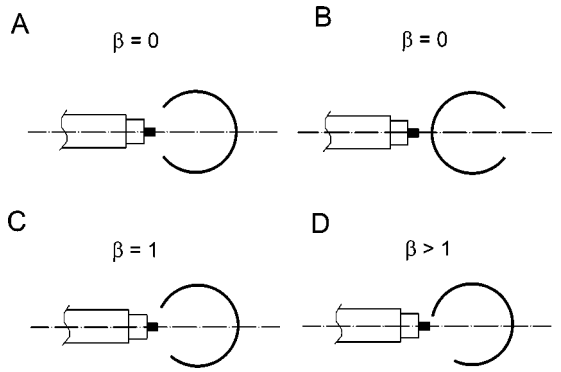

FIG. 2. Four positions of the folded strip with respect to the central conductor of the coaxial coupler corresponding to: (A) and (B) no coupling ($\beta = 0$), (C) critical coupling ($\beta = 1$), (D) overcoupling ($\beta > 1$).

PROBE PERFORMANCE

The evaluation of resonator parameters and the adjustment of resonator coupling were done using an extension of a well-known procedure which requires no equipment other than that already used in the pulsed spectrometer and which can be performed during experiments without the redirection of microwave input or output (*17, 19, 20*). Other methods for evaluating and adjusting resonator Q_U, Q_L, and the coupling coefficient β require the use of an expensive network analyzer, and the coupling adjustment requires at least a microwave sweep oscillator. With both of these setups, the microwave input or output must be redirected from the path taken during normal operation, requiring additional microwave components and potentially corrupting the tuning process; the following technique requires only a fast oscilloscope (>200 MHz) which is typically part of the spectrometer. Although aspects of this tuning procedure have been previously described (*17, 19, 20*), we include here a detailed discussion which incorporates a set of equations first derived by Ivannikov *et al.* (*19*) which are useful in resonator evaluation.

Figure 3 illustrates the magnitude of the reflected microwave power after the introduction of the pulse shown in Fig. 3A when the resonator is critically coupled (Fig. 3B) and overcoupled (Figs. 3C and 3D). It is clearly seen from the figure that the resonator behaves like a short circuit immediately after introduction of the microwave pulse and reflects the incident wave back toward the microwave source. Then power starts to penetrate into the resonator and the reflected power decreases exponentially. At equilibrium, corresponding to the middle part of the pulse, there is no net reflection since at critical coupling the resonator impedance matches the characteristic impedance of a waveguide or a coaxial line. When the microwave source is switched off, oppositely phased radiation is reflected which corresponds to power stored in the resonator and dissipated into the microwave line. (Because the diode detector is phase insensitive the phase change is not detected in the data displayed in Figs. 3B–3D. The appearance of oppositely phased radiation is marked with an arrow.) At overcoupling ($\beta > 1$, Figs. 3C and 3D), the reflected power increases initially (short circuit), then decreases, changes phase after crossing the zero point at time t_1, and increases (in absolute magnitude) again until it reaches its equilibrium level. The curves shown in Fig. 3 are easily recognized during the tuning process. As derived in Ref. (*19*) and discussed in the Appendix of this work, the power time dependence of the wave propagating back from the resonator (P_b) for the two dynamic processes corresponding to turning the microwave source on and off can be described by

$$P_{b,on}(t) = P_g\left(\frac{2\beta}{\beta+1}e^{-\omega t/2Q_L} + \frac{1-\beta}{1+\beta}\right)^2 \quad [1]$$

$$P_{b,off}(t) = P_g\frac{4\beta}{(\beta+1)^2}e^{-\omega t/Q_L} \quad [2]$$

$$Q_L = \frac{Q_U}{\beta+1},$$

where P_g is the microwave source power and Q_L and Q_U are loaded and unloaded resonator quality factors, respectively. For the critical coupling case ($\beta = 1$) both equations become equivalent and we obtain two identical curves as shown in Fig. 3B. Using these equations we can measure the resonator radiation damping time constant $\tau_R = Q_L/\omega$ and calculate the Q_L value. From Eq. [1] it can be derived that for the case of $\beta > 1$ time t_1 corresponding to the moment when reflected power equals zero is

$$t_1 = \frac{2Q_L}{\omega}\ln\frac{2\beta}{\beta-1}. \quad [3]$$

Now measuring t_1 from the first and τ_R from the second parts of the curve shown in Fig. 3C both Q_U and β can be calculated, even at overcoupling.

The entire measurement procedure can be performed during pulsed EPR operation without the rearrangement of spectrometer components and is useful for tuning and optimizing resonator characteristics for a given set of experimental conditions. For maximum echo amplitude in a pulsed EPR experiment for the case of broad inhomogeneous EPR lines, Mims derived an approximate condition $Q_L/\omega = t_p/4$, with t_p being a mw pulse width (*21*). Using this equation, a spin-echo experiment can be optimized by changing Q_L (via variation of β) and t_p.

The entire probe, including resonator and associated coupler, is very robust and does not suffer from microphonic effects. At the same time it has a simple design with parts that are relatively easy to fabricate. The range of available frequencies in the present configuration extends from 5 to 11 GHz using a set of different size Teflon resonator holders-A (Fig. 1A) which can accommodate sample tubes from 3.8 up to 5 mm. Figure 4 shows the dependence of the resonance frequency on the strip length for the 4- and 5-mm i.d. resonator assemblies (resonators

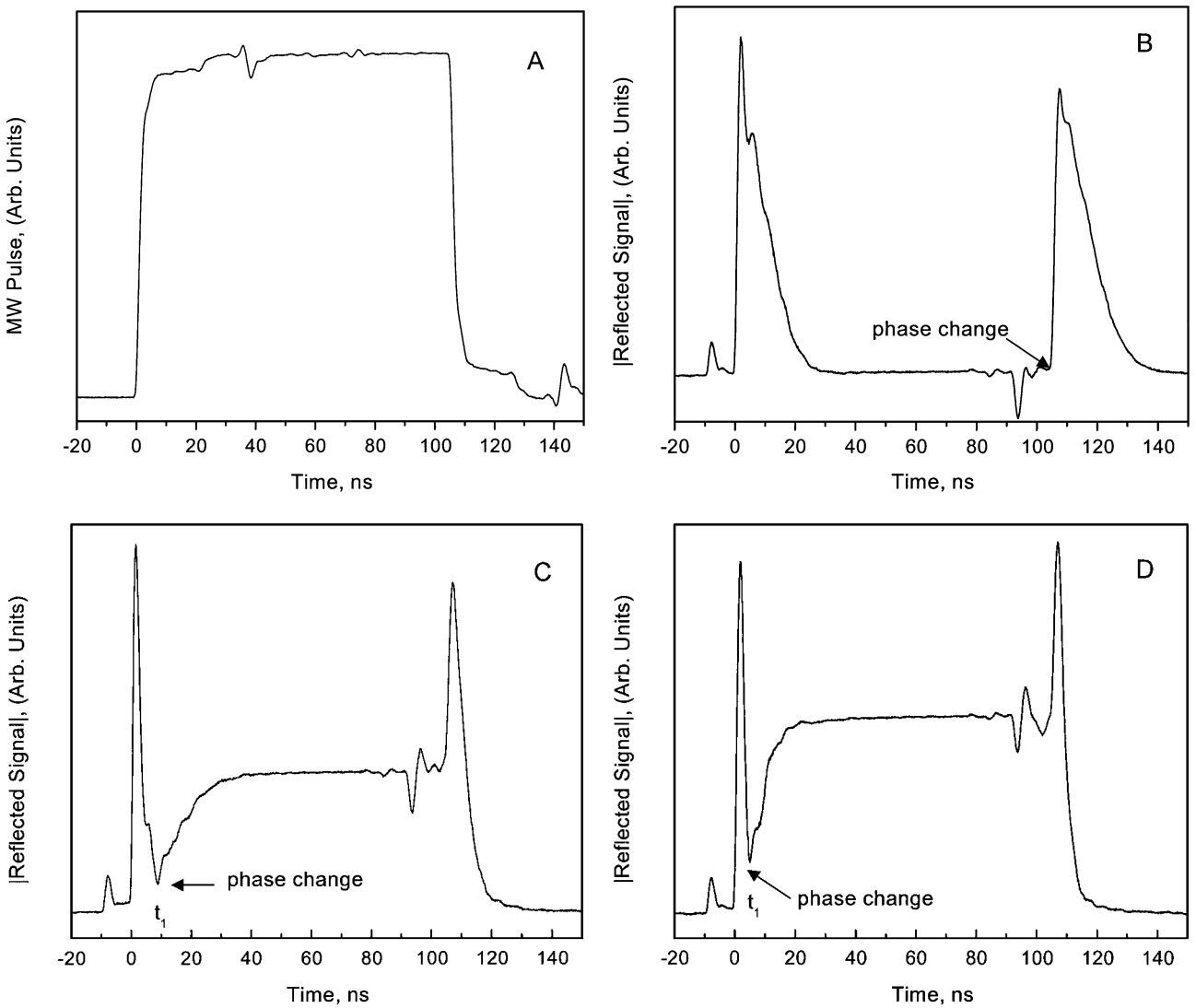

FIG. 3. Microwave dynamic radiation processes in the strip line resonator after introduction of a rectangular pulse. (A) The time dependence of the incident microwave signal. (B) The time dependence of the reflected microwave signal propagating back towards the source at critical coupling ($\beta = 1$, $\tau = 12.2$ ns, resonance frequency equal to 7.16 GHz) as shown in Fig. 2C. (C) The time dependence of the reflected microwave signal propagating back towards the microwave source at overcoupling ($\beta = 3.9$, $\tau = 5$ ns) as shown in Fig. 2D. (D) The same conditions as (C) but with a larger coupling coefficient ($\beta = 7$, $\tau = 3$ ns, 7.07 GHz). The measured Q_U value was 1100.

mounted in 4- and 5-mm i.d. Teflon holder-A). All resonant frequencies were measured at room temperature with quartz 4- and 5-mm EPR tubes inserted into the cavities. The available frequency range for the 4-mm resonator assembly extends from 6 to 11 GHz. Using the 5-mm-i.d. holder helps to decrease the lower limit to 5 GHz. At frequencies lower than 8 GHz (strip length more than 13 mm) the frequency dependence of the 4-mm assembly becomes nonlinear, which is probably caused by the end-to-end capacitance. Filling the EPR tube with water and decreasing the temperature to 4.2 K lower the resonant frequency by about 200–400 MHz. To reach frequencies higher than ~11 GHz, the strip length must be made too short to obtain acceptable filling factors and field homogeneity with 4-mm EPR tubes. This determines the upper frequency limit for the 4-mm resonator assembly. To make higher frequencies accessible it is possible to use sample tubes and corresponding holders of smaller diameter which restore acceptable filling factors and field homogeneity. The only change required is the construction of a smaller diameter Teflon holder-A (Fig. 1A) with the rest of the probe unaltered.

Figures 5A and 5B show the frequency dependence of the characteristic resonator radiation damping time constant τ_R and corresponding Q_L values for a series of resonators measured using the procedure described above. The resonators were mounted

on Teflon holders with inner diameters of 4 (●) or 5 mm (▲). A diode detector was used which was confirmed to have a linear response at the low incident microwave powers used in these measurements. The measured τ_R values vary from 17 to 2 ns. However, the leading and falling edges of the incident mw pulse have time constants of approximately 2 ns, and thus the values of τ_R determined at frequencies higher than 9.5 GHz (4-mm holders) were constrained by this limit.

The unloaded Q_U was measured at room temperature to be 900–1200 over the entire frequency range of the probe. The simple capacitive design allowed variation of the coupling coefficient β between a minimum of 0 and a maximum of 9 for the resonators tested. The maximum achievable coupling was dependent on both the resonator strip length and the diameter of the Teflon holder-A. For frequencies greater than 9 GHz, the maximum coupling of 9 could be achieved with the smaller diameter holder-A, producing the minimum measured Q_L (100) and τ_R(2 ns) values (Fig. 5, ●). As the frequency of the resonators was decreased by increasing the strip length, the maximum achievable coupling decreased, producing higher values of Q_L and τ_R.This is because as the strip length increases, the ends of the strip become closer together on the Teflon holder and thus restrict the range over which the resonator can be rotated to adjust the coupling (Fig. 2). The coupling maximum can be increased (and the corresponding Q_L and τ_R values decreased) at the lower frequencies by mounting the resonators on a larger diameter Teflon holder-A, which produces a larger separation of the resonator ends and increases the coupling range (Fig. 5, ▲). The upper frequency limit for this 5-mm resonator assembly, about 8–8.5 GHz, is determined by the filling factor and field homogeneity degradation as the strip length is decreased (see above).

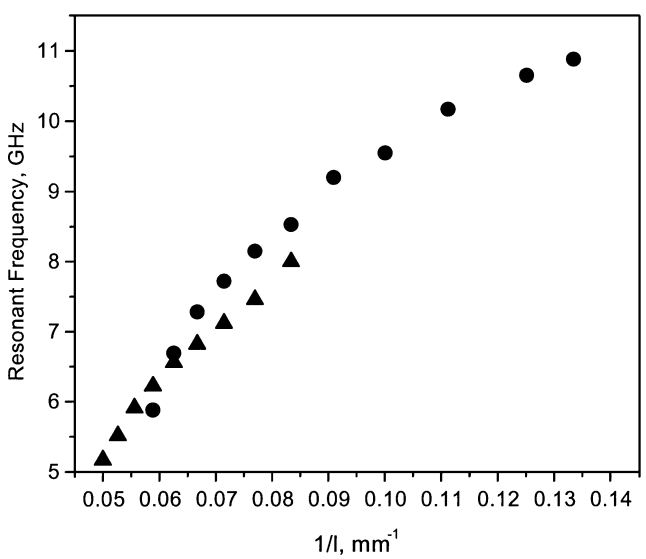

FIG. 4. The dependencies of the resonant frequencies of the 4- (●) and 5-mm (▲) strip line resonator assemblies on their strip lengths.

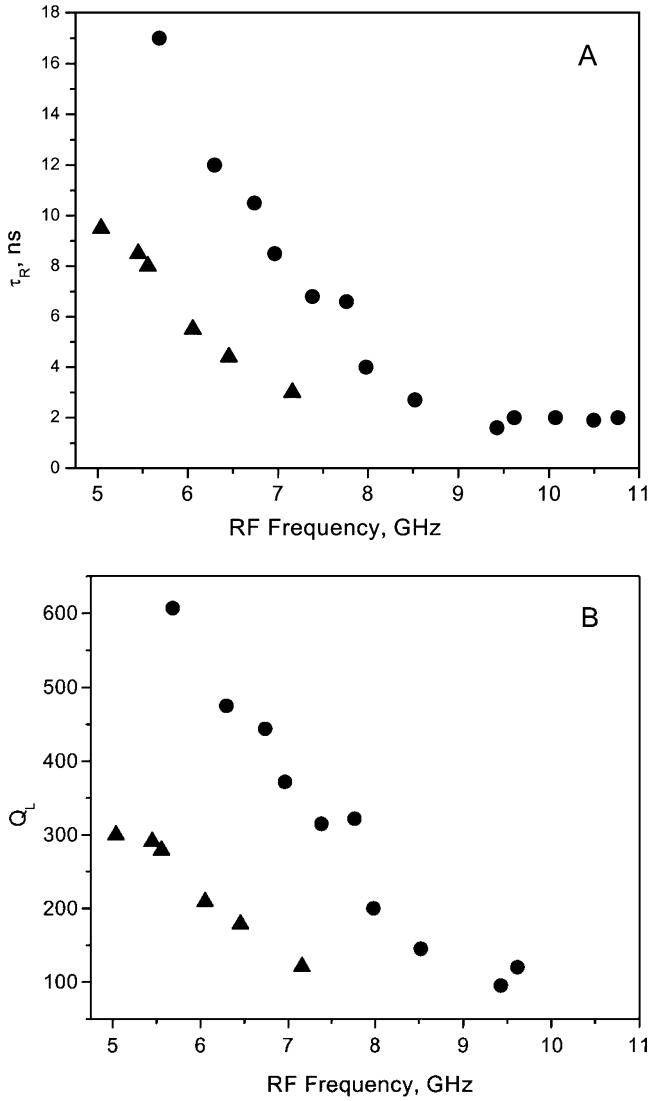

FIG. 5. The resonant frequency dependencies of τ and Q_L measured for the 4- (●) and 5-mm (▲) strip line resonator assemblies.

The resonator conversion factor Λ is defined as $\Lambda = B_1/\sqrt{P}$, where B_1 is the amplitude of the microwave magnetic field in the laboratory reference frame and P is the power applied at the resonator. The value of Λ was measured to be $4(G/\sqrt{W})$ at 9.1 GHz for the 4-mm resonator assembly, which compares favorably with other resonator designs. Experiments indicate that Λ does not deviate substantially from this value until the resonance frequency reaches the upper limit of 11 GHz for this diameter holder.

PULSED ENDOR

For pulsed ENDOR experiments the design was modified to accommodate an RF coil. The coil wound of 30-gauge silver wire was mounted on top of the Teflon holder-B which is 11 mm in

diameter and held in place by Teflon heat shrink tubing. The coil consists of 12 turns put in grooves threaded at 44 threads per inch on the Teflon surface. Two 6-turn sections of the coil are separated by 2.5-mm clearance for the central wire of the capacitive coupler to insert. The inductance of the coil in the presence of the microwave shield measured 0.8 μH and the self–resonance frequency of the coil measured at the same conditions was about 95 MHz. To prevent attenuation of the RF field by eddy currents, the microwave shield consisted of two vertically cut pieces with no electrical contact between them. With a thin (about 0.1 mm) Teflon film inserted between the shield halves the measured capacitance was 17 pF, which presents a short circuit for a microwave (~9GHz) current and a substantial resistance for an RF (<100 MHz) current. As a result of cutting the microwave shield, the Q_U of the resonator decreased by about 35–40%. There was also a measured RF field decrease of about 35–40% due to eddy currents in the microwave shield. To estimate the amplitude of the RF field we ran a Mims type ENDOR experiment at room temperature, 9.5 GHz using BDPA (α,γ-bisdiphenylene-β-phenylallyl) radical doped into polystyrene as a test system. From the RF pulse length (14 μs) corresponding to the 180-degree proton pulse we estimated the amplitude of the RF field to be 8 G in the rotating reference frame with 200 W RF power applied using the matching network described below.

The RF power feed consisted of a single stainless steel coaxial cable (o.d. 141 in.) of 100-cm length with its central wire connected to the one-coil terminal. The shield of the coax was connected to the resonator body serving as a ground terminal. The matching circuit we used (*22*) is shown in Fig. 6. The resistors and capacitors were mounted outside the cryostat at the top of the probe. With a capacitance value of 400 pF the input impedance deviation was less than 20% up to 30 MHz. Measurements were done using an HP4815A RF vector impedance meter. Since the RF amplifier (200L Amplifier Research, 200 MHz bandwidth, 200 W output power) is tolerant to 100% mismatch, it can be beneficial to use no matching at all. In this case one could get as much as twice the RF field (up to 16 G in the rotating reference frame). However, a slowly decaying reflected wave randomly modulates the echo phase due to the presence of the RF field component parallel to the constant magnetic field. To avoid this effect, the RF pulse must be moved away from the microwave pulse and the echo signals. This is inconvenient for those experiments where it is useful to apply short 180-degree RF pulses. Thus, depending on the experimental conditions required, the RF may be provided either with or without a matching network.

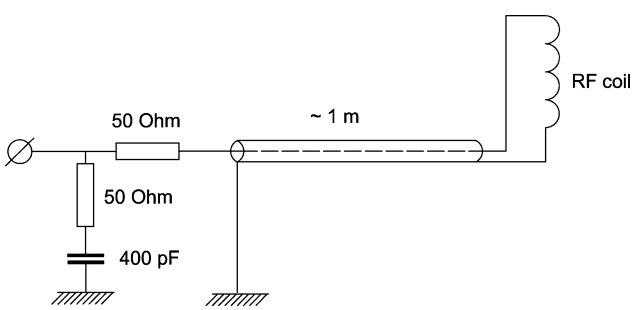

FIG. 6. The RF coil matching network used in pulsed ENDOR experiments.

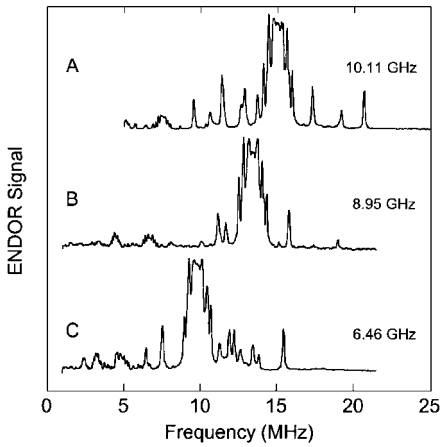

FIG. 7. Multifrequency Mims-type ENDOR spectra of Cu(II) impurity in a single crystal of GlyGly. Experimental parameters for all spectra: temperature = 4.2 K; 90° EPR pulse width = 20 ns; RF pulse length = 9.4 μs; RF power ~200 W; repetition rate = 60 Hz; RF frequency increment 20 kHz. (A) ν_{epr} = 10.11 GHz; τ = 300 ns; magnetic field B_0 = 353.9 mT; the spectrum is an average of 5 scans with 30 echoes averaged per point. (B) ν_{epr} = 8.95 GHz; τ = 270 ns; B_0 = 315.7 mT; average of 5 scans with 30 echoes averaged per point. (C) ν_{epr} = 6.46 GHz; τ = 300 ns; B_0 = 230.8.7 mT; average of 8 scans with 30 echoes averaged per point.

A set of multifrequency Mims-type pulsed ENDOR spectra from a Cu(II) impurity in a single crystal of GlyGly is displayed in Fig. 7. The peaks in the spectra are derived from hyperfine coupling to both hydrogen and nitrogen, and thus their frequencies exhibit different EPR excitation frequency dependence (and corresponding static magnetic field dependence) which can aid in their spectral assignment.

SUMMARY

The design, construction, and performance of a multifrequency pulsed EPR/ENDOR probe have been presented. The primary benefits of the probe include robust, easily adjustable capacitive coupling, which allows the achievement of optimal Q_L values for pulsed experiments; simplicity of construction; a broad EPR excitation frequency range of 5–11 GHz; and incorporation of ENDOR capabilities without significant degradation of resonator characteristics.

APPENDIX

Equation [1] was obtained rigorously from the first principles in Ref. (*19*) via the solution of differential equations. By incorporating a basic assumption not made in Ref. (*19*) we obtain a simpler derivation which provides physical insight into

the dynamic processes of the reflected microwave pulse power. This assumption is that the growth and decay of the field inside of the resonant cavity during ($E_{c,on}$) and after ($E_{c,off}$) the introduction of a microwave pulse follow exponential behavior, such that

$$E_{c,off} = E_o e^{-t/\tau_R}$$
$$E_{c,on} = E_o(1 - e^{-t/\tau_R}).$$

To determine the E_0 value let us consider the equilibrium conditions

$$P_g = P_b + P_{in}, \qquad P_b = \Gamma^2 P_g, \qquad \Gamma = \frac{1-\beta}{1+\beta}$$

in which P_g is source power, P_b is the reflected power, P_{in} is the power admitted into the resonator, and Γ is the reflection coefficient. From these equations we obtain

$$P_{in} = P_g(1 - \Gamma^2) = P_g \frac{4\beta}{(1+\beta)^2}.$$

Assuming $P \sim \alpha E^2$, where α is an arbitrary proportionality coefficient, we obtain the time dependence for P_{in} and E_c inside of the cavity:

$$P_{in}(t) = P_g \frac{4\beta}{(1+\beta)^2}\left(1 - e^{-t/\tau_R}\right)^2, \qquad E_{c,on}(t) = \frac{\sqrt{P_{in}(t)}}{\sqrt{\alpha}}.$$

To obtain the time-dependent reflected power $P_{b,on}(t)$ we take into account

$$P_{b,on}(t) = \alpha(E_g - E_{out}(t))^2, \qquad P_{out}(t) = \frac{\beta\omega U(t)}{Q_U},$$
$$U(t) = \frac{P_{in}(t) Q_U}{\omega}$$

in which E_{out} is the field in the waveguide after the microwave source is switched off, U is the energy stored in the cavity, and $P_{out} = \alpha E_{out}^2$. After some algebra we obtain

$$P_{b,on}(t) = P_g\left(\frac{2\beta}{1+\beta}e^{-t/\tau_R} + \frac{1-\beta}{1+\beta}\right)^2.$$

ACKNOWLEDGMENTS

N.I.A. thanks Dr. J. Peisach for constant encouragement in pursuing this work and Dr. A. V. Koptyug for helpful discussions. This work was supported by Grants GM60609 (G.J.G.) and GM40168 (J.P.) from the National Institutes of Health.

REFERENCES

1. D. J. Singel, Multifrequency ESEEM: Perspectives and applications, *in* "Advanced EPR: Applications in Biology and Biochemistry" (A. J. Hoff, Ed.), pp. 119–133, Elsevier, Amsterdam (1989).
2. B. M. Hoffman V. J. DeRose, P. E. Doan, R. J. Gurbiel, A. L. P. Houseman, and J. Telser, Metalloenzyme active-site structure and function through multifrequency CW and pulsed ENDOR, *in* "Biol. Magn. Reson." (L. J. Berliner and J. Reuben, Eds.), pp. 151–218, Plenum, New York (1993).
3. H. L. Flanagan and D. J. Singel, Analysis of ^{14}N ESEEM patterns of randomly oriented solids, *J. Chem. Phys.* **87,** 5606–5616 (1987); A. Lai, H. L. Flanagan, and D. J. Singel, Multifrequency electron spin echo envelope modulation in S = 1/2, I = 1/2 systems: Analysis of the spectral amplitudes, line shapes and linewidths, *J. Chem. Phys*. **89,** 7161–7166 (1988); E. J. Reijerse and S. A. Dikanov, Electron spin echo envelope modulation spectroscopy on orientationally disordered systems: Line shape singularities in S = 1/2, I = 1/2 spin systems, *J. Chem. Phys*. **95,** 836–845 (1991); E. J. Reijerse, A. M. Tyryshkin, and S. A. Dikanov, Complete determination of nitrogen quadrupole and hyperfine tensors in an oxovanadium complex by simultaneous fitting of multifrequency ESEEM powder spectra, *J. Magn. Reson*. **131,** 295–309 (1998).
4. W. B. Mims and J. Peisach, Water coordination by heme iron in metmyoglobin, *J. Biol. Chem*. **259,** 2704–2706 (1984); S. C. Larsen and D. J. Singel, Multifrequency ESEEM spectroscopy of ammonia adsorbed on silica-supported reduced molybdenum oxide, *J. Phys. Chem*. **96,** 10594–10597 (1992); S. A. Dikanov and Y. D. Tsvetkov, "Electron Spin Echo Envelope Modulation Spectroscopy," CRC Press, Boca Raton (1992); B. E. Sturgeon, J. A. Ball, D. W. Randall, and D. R. Britt, ^{55}Mn electron spin echo ENDOR of Mn^{2+} complexes, *J. Phys. Chem*. **98,** 12871–12883 (1994).
5. D. J. Singel and H. L. Flanagan, Multifrequency ESEEM *in* "Pulsed EPR: A New Field of Applications" (C. P. Keijzers, E. J. Reijerse, and J. Schmidt, Eds.), pp. 108–113, North-Holland, Amsterdam (1989); R. G. Evelo, A. J. Hoff, S. A. Dikanov, and A. M. Tyryshkin, An ESEEM study of the oxidized electron donor of plant photosystem. II. Evidence that D is a neutral tyrosine radical, *Chem. Phys. Lett*. **161,** 479–484 (1989); R. B. Clarkson, D. R. Brown, J. B. Cornelius, H. C. Crookham, W.-J. Shi, and R. L. Belford, S-band electron spin echo spectroscopy, *Pure Appl. Chem*. **64,** 893–902 (1992).
6. W. B. Mims and J. Peisach, ESEEM and LEFE of metalloproteins and metal compounds, *in* "Advanced EPR: Applications in Biology and Biochemistry" (A. J. Hoff, Ed.), pp. 1–57, Elsevier, Amsterdam (1989); G. J. Gerfen, B. F. Bellew, and D. J. Singel, Line-narrowing in electron spin echo envelope modulation spectroscopy: Determination of the ^{15}N hyperfine interaction parameters of para-nitrobenzo-^{15}N-nitrile radical anion in frozen solution, *Chem. Phys. Lett*. **180,** 490–496 (1991); G. J. Gerfen and D. J. Singel, Determination of hyperfine interaction matrix principal values and principal axis orientations in an orientationally disordered solid: A multifrequency electron spin echo envelope modulation study of nitrogen-15 in a copper(II)-^{15}N-imidazole complex, *J. Chem. Phys*. **100,** 4127–4137 (1994); S. A. Dikanov, A. P. Spoyalov, and J. Hüttermann, Exploiting the properties of line-shape singularities in orientationally selected electron spin echo envelop modulation spectra of Cu^{2+}(^{15}N-imidazole)$_4$ for determination of hyperfine coupling with the remote imidazole nitrogen, *J. Chem. Phys*. **100,** 7973–7983 (1994).
7. H. J. Schneider and P. Dullenkopf, Slotted tube resonator: A new NMR probe head at high observing frequencies, *Rev. Sci. Instrum*. **48,** 68–73 (1977); M. Mehring and F. Freysoldt, A slotted tube resonator STR for pulsed ESR and ODMR experiments, *J. Phys. E* **13,** 894–895 (1980).
8. W. N. Hardy and L. A. Whitehead, Split-ring resonator for use in magnetic resonance from 200-2000 MHz, *Rev. Sci. Instrum*. **52,** 213–216 (1981); W. Froncisz and J. S. Hyde, The loop-gap resonator: A new microwave

lumped circuit ESR sample structure, *J. Magn. Reson.* **47,** 515–521 (1982); R. A. Venters, J. R. Anderson, J. F. Cline, and B. M. Hoffman, ENDOR with a loop-gap resonator, *J. Magn. Reson.* **58,** 507–510 (1984).

9. J. S. Hyde and W. Froncisz, Loop gap resonators, *in* "Advanced EPR: Applications in Biology and Biochemistry" (A. J. Hoff, Ed.), pp. 277–305, Elsevier, Amsterdam (1989).
10. B. T. Ghim, R. W. Quine, S. S. Eaton, and G. R. Eaton, Design and fabrication of copper-film loop-gap resonators, *J. Magn. Reson. A* **120,** 72–76 (1996); M. Alecci, I. Nicholson, and D. J. Lurie, A novel multiple-tuned radiofrequency loop-gap resonator for use in PEDRI, *J. Magn. Reson. B* **110,** 82–86 (1996).
11. S. Pfenninger, J. Forrer, and A. Schweiger, Bridged loop-gap resonator: A resonant structure for pulsed ESR transparent to high frequency radiation, *Rev. Sci. Instrum.* **59,** 752–760 (1988); J. Forrer, S. Pfenninger, J. Eisenegger, A. Schweiger, and Th. Weiland, A pulsed ENDOR probehead with bridged loop-gap resonator: Construction and perfomance, *Rev. Sci. Instrum.* **61,** 3360–3367 (1990); V. Weis, W. Mittelbach, J. Claus, K. Möbius, and T. Prisner, Probehead with interchangeable tunable bridged loop-gap resonator for pulsed zero-field optically detected magnetic resonance experiments on photoexcited triplet states, *Rev. Sci. Instrum.* **68,** 1980–1985 (1997).
12. A. Sienkiewicz, K. Qu, and C. P. Scholes, Dielectric resonator-based stopped-flow electron paramagnetic resonance, *Rev. Sci. Instrum.* **65,** 68–74 (1994).
13. B. Johansson, S. Haraldson, L. Pettersson, and O. Beckman, A stripline resonator for ESR, *Rev. Sci. Instrum.* **45,** 1445–1447 (1974); J. L. Davis and W. B. Mims, ENDOR cavity for electron spin echo experiments, *Rev. Sci. Instrum.* **49,** 1095–1097 (1978).
14. C. P. Lin, M. K. Bowman, and J. R. Norris, A folded half-wave resonator for EPR spectroscopy, *J. Magn. Reson.* **65,** 369–374 (1985).
15. A. V. Koptyug, E. J. Reijerse, and K. A. Klaassen, New transmission line resonator for pulsed EPR, *J. Magn. Reson.* **125,** 369–371 (1997).
16. W. B. Mims, Electron spin echoes, *in* "Electron Paramagnetic Resonance" (S. Geschwind, Ed.), pp.263–351, Plenum, New York (1972); J. Forrer, S. Pfenninger, B. Wagner, and Th. Weiland, Progress in instrumentation for pulsed EPR and ENDOR spectroscopy, *Pure Appl. Chem.* **64,** 865–872 (1992).
17. G. A. Rinard, R. W. Quine, S. S. Eaton, G. R. Eaton, and W. Froncisz, Relative benefits of overcoupled resonators vs inherently low-Q resonators for pulsed magnetic resonance, *J. Magn. Reson. A* **108,** 71–81 (1994); S. Pfenninger, W. Froncisz, J. Forrer, J. Luglio, and J. S. Hyde, General method for adjusting the quality factor of EPR resonators, *Rev. Sci. Instrum.* **66,** 4857–4865 (1995).
18. Yu. Grishin, C. W. M. Kay, A. A. Doubinskii, and K. Mobius, A novel loop-gap resonator probehead for EPR and ENDOR at X-band, *Appl. Magn. Reson.* **13,** 387–392 (1997); R. D. Britt, and M. P. Klein, A versatile loop-gap resonator probe for low-temperature electron spin-echo studies, *J. Magn. Reson.* **74,** 535–540 (1987).
19. V. I. Ivannikov, Yu. D. Chernousov, and I. V. Shebolaev, Ob ustanovlenii kolebani v resonatore, *Vopr. Atomn. Nauk. Tech.* **6,** 55–58 (1989).
20. M. Willer, J. Forrer, J. Keller, S. van Doorslaer, and A. Sweiger, S-band (2-4 GHz) pulse electron paramagnetic resonance spectrometer: Construction, probe head design, and performance, *Rev. Sci. Instrum.* **71,** 2807–2817 (2000).
21. W. B. Mims, Electron echo method in spin resonance spectrometry, *Rev. Sci. Instrum.* **36,** 1472–1479 (1965).
22. M. Peric and A. Dulcic, Simple matching for NMR coils in ENDOR spectrometers, *J. Phys. E* **14,** 700–701 (1981).